METEOROLOGICAL APPLICATIONS
Meteorol. Appl. **18**: 111–122 (2011)
Published online 16 August 2010 in Wiley Online Library
(wileyonlinelibrary.com) DOI: 10.1002/met.219

Climate change and its human dimensions based on GIS and meteorological statistics in Pearl River Delta, Southern China

Haoyang Dou[a,b] and Xinyi Zhao[a]*
[a] *College of Urban and Environmental Sciences, Peking University, Beijing, China*
[b] *The Key Laboratory for Environmental and Urban Sciences, Shenzhen Graduate School, Peking University, Shenzhen, Guangdong, China*

ABSTRACT: Climate change in the Pearl River Delta (PRD) has attracted growing attention along with rapid urbanization in Southern China. Annual mean temperatures in this area have increased more rapidly than the average level, which can be attributed to population expansion and land use changes in this region.

In this study, temperature records from 31 weather stations in the PRD in Guangdong, China and the global dataset from the National Centres for Environmental Prediction (NCEP) Reanalysis (R-2) are analysed. Data from NCEP R-2 and temperature soundings taken at 850 hPa are used to define the background temperature. Anthropogenic temperature is then calculated according to the observed temperature and background temperature. The relationships of anthropogenic temperature to population density and area ratio of land-use types are analysed by univariate and multiple regression analysis techniques.

Spatial distribution of anthropogenic temperature in the daytime is different from that at night. Model results indicate that relationships between population and anthropogenic temperature in the daytime are logarithmic or inverse but tend to be linearly related at night. Multiple regression analysis conducted on the area ratios of land-use types and anthropogenic temperature shows that a strong relationship exists between the two in spring and autumn. Positive correlations with anthropogenic temperature from arid land, water bodies and urban land, as well as a negative correlation from woodland, are detected regardless of time of day. Contrary to the paddy field, grassland and sea show a negative correlation with anthropogenic temperature in the daytime and a positive correlation at night.

KEY WORDS anthropogenic temperature; land-use type; population density; statistical analysis

Received 5 September 2009; Revised 14 May 2010; Accepted 26 May 2010

1. Introduction

Global and regional climate change has received increasing attention in recent years and has been widely studied by many researchers for several decades. Apart from natural factors, climate change is also affected by anthropogenic factors (i.e. human dimensions) such as increased greenhouse gases generated from fossil fuel burning and land use cover change (LUCC). The relationship between anthropogenic factors and climate change is becoming a popular topic in the field of climate change research.

Since 1978, China has experienced high-speed urbanization, which has significantly affected local climate. Urban heat resulting from traffic, greenhouse gas emissions and human activities is prevented from being released into the atmosphere by tall buildings, thus contributing to the formation of an urban microclimate characteristic of an urban heat island (UHI). Unger *et al.* (2001) constructed horizontal isotherm maps to show the average spatial distribution of maximum UHI intensity and found that the isotherms of maximum UHI intensity increase in regular concentric shapes from the outskirts to central urban areas. Models were also built to describe the quantitative effects of anthropogenic and natural factors on urban-rural temperature differences. Proximity to the city centre and large urban built-up area were shown to play important roles in urban temperature increment. In connection with high air pollution levels, increasing temperature arising from UHI contributes to increased thermal discomfort, which adversely affects the comfort and health of city inhabitants (Piotrowicz, 2009). Heat waves and hot nights may lead to bad moods in city dwellers. They become prone to fatigue, lethargy or insomnia, concentration deficiency, dispiritedness and apathy, lack of appetite, and persistent headaches or frequent migraines (Hessman-Konsaris, 1998). The impact of climate change on human health is complex and significant. In addition to increased risk of mental disorders, climate change may also affect the occurrence of cancers, cardiovascular and respiratory disease, and other heat-related illnesses (Rosenthal and Jessup, 2009).

Yilmaz *et al.* (2009) concluded that human activities associated with urbanization contribute to global warming in two ways: (1) by changing natural Earth surfaces and causing these to store more heat in urban areas,

* Correspondence to: Xinyi Zhao, College of Urban and Environmental Sciences, Peking University, Beijing, China.
E-mail: sh-zhao@urban.pku.edu.cn

and, (2) by producing more than normal levels of carbon for excessive heat storage. The LUCC causes variations in ground-level absorption of solar radiation through changes in surface albedo, roughness, water vapour exchange and soil thermal properties. These changes, in turn, affect sensible and latent heat fluxes. As population increases, people progressively consume greater amounts of fossil fuel and increasingly engage in harmful activities, such as deforestation and production of carbon dioxide and other greenhouse gases.

The degree of urbanization can be revealed by properties such as construction activities, motor vehicles, energy consumption and population. Among these factors, the population of a city may be selected as an important indicator of urbanization. Although rapid population increase might accelerate urbanization, the relation between population movement from rural areas to the suburbs of modern cities and increasing energy flow may also be important (Tonkaz and Centin, 2007). Many researchers believe regional population growth has led to urban warming and a logarithmic relationship exists between population density and temperature (Jenerette *et al*., 2007; Tonkaz and Centin, 2007; Yilmaz *et al*., 2009). Oke (1973) and Du *et al*. (2007) studied the impact of urban expansion on regional temperature change and found that UHI intensity and logarithm of total urban population are credibly correlated. Research conducted in Turkey indicated that the relationships between population growth and maximum temperature and between the number of vehicles and minimum temperature are statistically significant (Yilmaz *et al*., 2009). In the study of Stanhill and Kalma (1995), solar radiation in Hong Kong decreased by more than one-third between 1960 and 1995 while the population doubled and total use of fossil fuels increased more than sevenfold, causing a decline in irradiance and an increase in anthropogenic heat production. The relationship between spatial distribution of population and temperature has been shown to be insignificant thus far. However, Karl *et al*. (1988) pointed out that annual mean temperatures for the United States at stations in populated areas of 10 000 people or more were 0.1 °C higher than those in nearby stations located in rural areas with populations less than 2000. Jenerette *et al*. (2007) reported a weak relationship between population density and mean surface temperature using bivariate linear regression analysis. They showed that surface temperature variation within census tracts decrease by 0.45 °C for each additional 1000 residents km^{-2}.

Industrialization and population growth have accelerated temperature increase through expanded human activities, especially land use (Jin *et al*., 2005). As one of the most visible results of human modification on the terrestrial ecosystem, LUCC has a significant impact on local, regional and global climate (Weng, 2001). The changes in LUCC widen the temperature difference between urban and rural areas. Lin *et al*. (2008) pointed out that Taichung and two other smaller nearby cities in Taiwan clearly show higher temperatures than those over mountains and farmlands. The temperature at the centre of Taichung is about 5 °C higher than that over the forested mountain area to the east and the rice paddies to the west. The change in land surface temperature is mainly associated with changes in construction materials in the urban area and in vegetation abundance in both urban and rural areas (Xiao and Weng, 2007). Land use is a key determinant of variations in exposure to temperature. For example, multi-storey buildings and materials used in pavement and construction could affect temperature exposure at the microscale (Harlan *et al*., 2006).

Some researchers have used the Observation Minus Reanalysis (OMR) method to estimate the impact of urbanization on climate. They computed the difference between the trends of surface temperature observations (which reflect all climate forcing, including natural and anthropogenic effects from the surface) and the NCEP/NCAR Reanalysis (NNR) surface temperatures, which are only influenced by assimilated atmospheric temperature trends (Kalnay and Cai, 2003; Kalnay *et al*., 2006). The OMR method was recently applied by Zhou *et al*. (2004) to estimate the impact of urbanization over southeastern China during the last two decades when rapid economic growth took place. The estimated increase of mean winter surface temperature was 0.05 °C *per* decade, which was computed using OMR. Lim *et al*. (2005) showed that the OMR trend (i.e. surface temperature trend difference between observation and NNR data) has a strong dependence on the type of land (determined using MODIS). They found that the results using NNR were similar to those using the European Centre for Medium Range Weather Forecasts 40 year Reanalysis (ERA-40). However, the surface temperature trend difference obtained from the OMR method is not only due to urbanization effects, including LUCC, but is also a result of changes in agricultural practices, such as irrigation and deforestation, and the effects of near-surface aerosols and precipitation changes associated with both urbanization and industrialization (Kalnay *et al*., 2006).

The purpose of the present study is to construct isotherm maps to show the spatial distribution of anthropogenic temperature in the studied area and analyse the relationship between anthropogenic temperature and human dimensions (population density and area ratio of land-use type). Seasonal and diurnal variations of these relationships are also examined.

2. Study area and data

The Pearl River Delta (PRD) along the coast of the South China Sea is selected as the study area because of its rapid urbanization since China's economic reform and Open Door policy started in late 1978. It is located in the south of Guangdong Province and is called the PRD Economic Region, which includes nine cities at the prefecture level, according to the economic development program established by the Guangdong provincial government in 1994. These cities are Guangzhou, Shenzhen, Zhuhai,

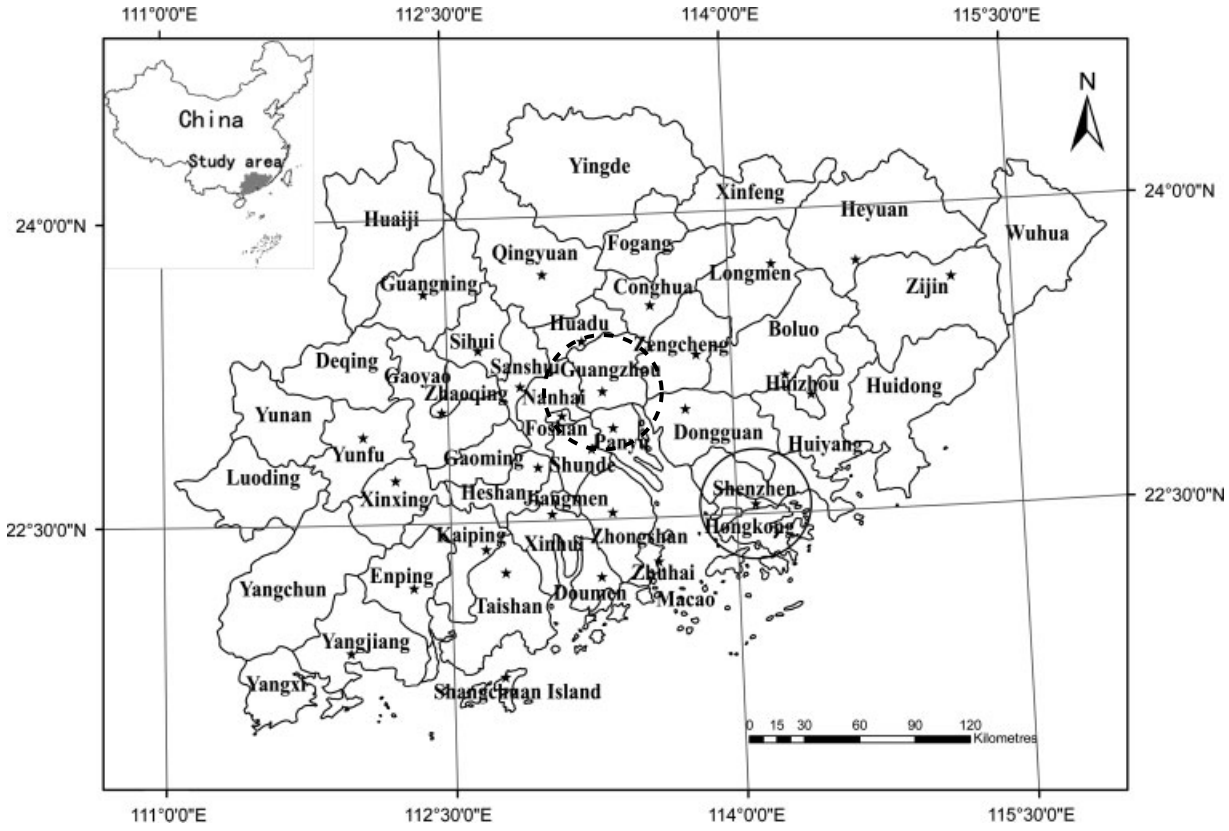

Figure 1. Geographical location and control units of the PRD. Note that inland units and coastal units are control units centred at the 31 conventional weather stations (five-pointed star) with a radius of 30 km. Inland unit example: dashed circle; coastal unit example: solid circle.

Foshan, Jiangmen, Dongguan, Zhongshan, Huizhou and Zhaoqing (Figure 1). The area of PRD is more than 41 700 km^2, which is 0.4% of the entire country with about 40 million residents. This area is bordered by Luoping Mountain to the west and north, and Luofu Mountain to the east. Pearl River, the primary water system of the PRD, consists of the Xi River, Bei River, and Dong River. The study area is of subtropical humid monsoon climate and has good hydrothermal condition. The flood season is from April to September and the dry season is from October to March. Most large cities in this area are situated on the plain of estuarine delta.

Thirty one districts in the PRD region are included in this study, eight of which (Taishan, Zhongshan, Doumen, Zhuhai, Dongguan, Shenzhen, Yangjiang, and Shangchuan Island) are off the coast (Figure 1). This densely populated region is among the first regions opened to the outside world when China started its economic reform, and it has experienced rapid urbanization since the 1980s (Chen *et al*., 2006). Based on a Landsat TM (Thematic Mapper) data image received in December 2002, a multi-band image is synthesized by TM2-4 bands. Unsupervised classification is first used in the remote sensing image, followed by manual interpretation to determine 20 land-use types. The resolution of the remote sensing image is 30 m. According to land use properties, the data are reclassified into seven categories: paddy field, arid land, woodland, grassland, water body, urban land and rural residence. Paddy field and woodland are dominant in the study region, except in the Pearl River estuary where there is a large area ratio of urban land because of the existence of large cities (Figure 2).

This paper is based on the data of daily maximum and minimum temperatures (regarded as the temperature in the daytime and at night) from 31 conventional weather stations located in 31 districts in the PRD region for each month of 2002. Data taken at 850 hPa at Lianping, Shantou, Yangjiang and Hong Kong, as well as gridded data of global NCEP R-2 from 1980 to 2005, are used to determine background temperature. Resident population data for the counties in 2002 from the Guangdong Yearbook are used to analyse the relationship between population and the anthropogenic temperature.

3. Spatial analysis

As shown in Figure 1, the dashed and solid circle are two control units made with a radius of 30 km, centred at Guangzhou and Shenzhen, as examples of the 31 conventional weather stations (see also Appendix A). The temperature for each station is affected by land use pattern and population distribution in the control unit.

3.1. Area ratio of land-use types

Land-use types, such as low-density grasslands and beaches, rarely appear and are thus ignored and merged

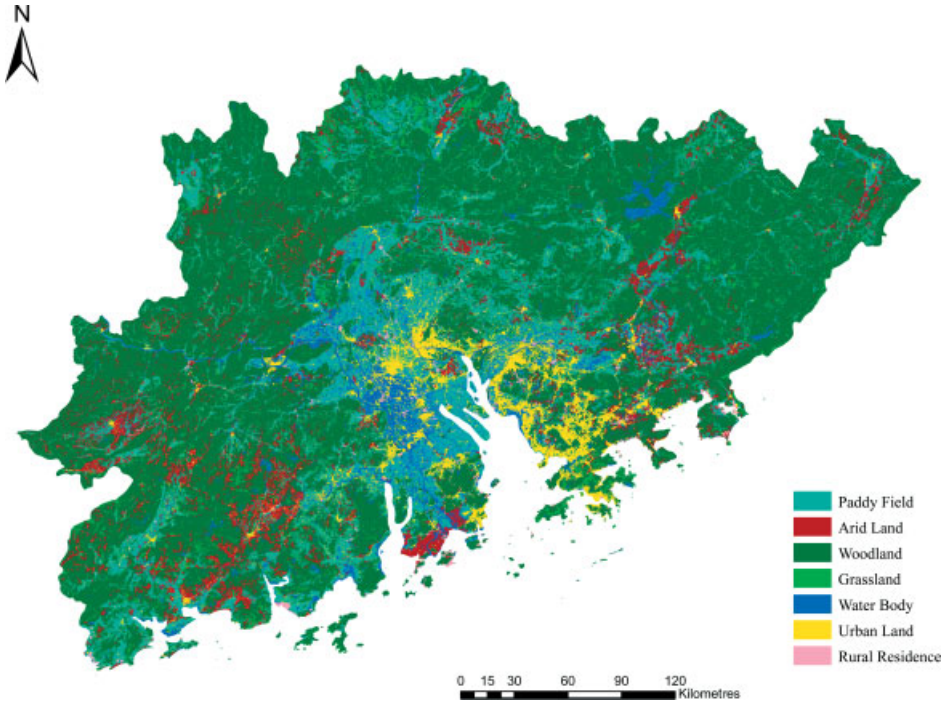

Figure 2. Land use map of the PRD. It is based on Landsat TM (Thematic Mapper) data image received in December 2002. According to land use property, the data are reclassified into seven categories: paddy field, arid land, woodland, grassland, water body, urban land, and rural residence.

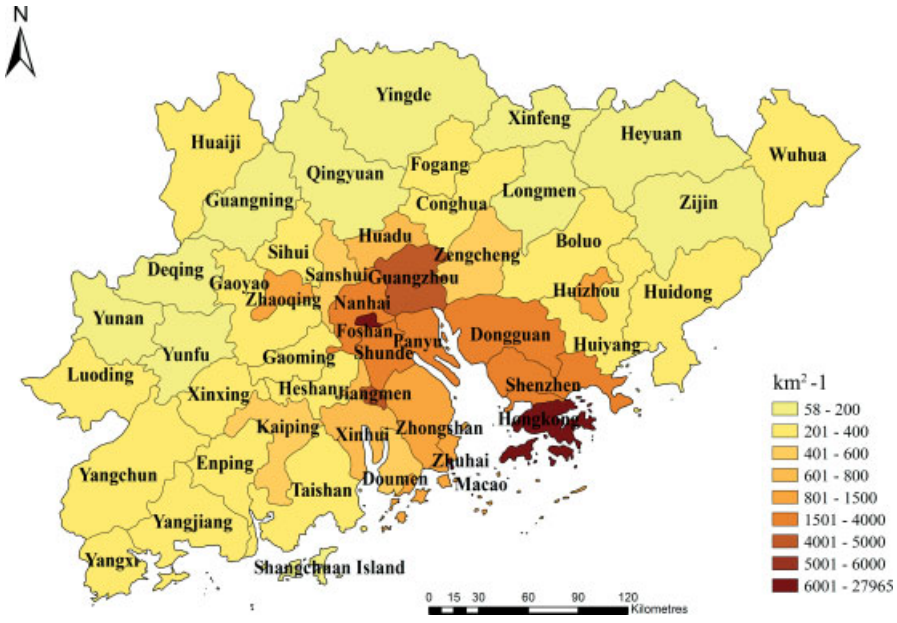

Figure 3. Population density of the PRD (km^{-2}).

into other types. Sea is considered a land-use type because of its great influence on the climate nearby. The area ratio of each land-use type is calculated using Equation (1):

$$TP_i = \frac{S_i}{A} \ (i = 1, 2, \ldots, n) \tag{1}$$

TP_i is the area ratio of each land-use type in each control unit; S_i is the area of each land-use type; A is the area of the control unit, and n is the number of land-use type in each control unit.

3.2. Population density

Apart from the selected 31 districts, 20 counties around it are involved and were converted to raster images for the calculation of population density in control units (Figure 3). The area of raster corresponding to different values of population density in each control unit was

calculated and the ratio of the raster area to the total area of the control unit was taken as the weight. The weighted average shown in Equation (2) is the population density of each control unit:

$$D = \sum_{j=1}^{k} \frac{N_j}{N} \times PD_j \ (j = 1, 2, \ldots, k) \qquad (2)$$

D is the population density in each control unit; N_j is the number of rasters corresponding to different values of population density; N is the total number of rasters in a control unit; PD_j is the population density in each county included in each control unit, and k is the number of counties in each control unit.

4. Anthropogenic temperature

Based on the research of the atmospheric boundary layer of the PRD (Fan *et al*., 2005), temperature variability at 850 hPa, which approximately reaches the top of the atmospheric boundary layer, is not affected by urban anthropogenic heat. The temperature tendency in Equation (B3) is calculated using the data of Lianping, Yangjiang, Shantou, and Hong Kong at the altitude of 850 hPa from 1980 to 2005, because the data for the four upper-air stations are in the global data exchange.

Since the temperature data of upper-air stations at the altitude of 1000 hPa in atmospheric boundary layer are affected by anthropogenic emissions, NCEP R-2 data are used to reflect the natural temperature variability. The difference in temperature tendency of a grid point (22.5 °N, 112.5 °E) from the NCEP R-2 dataset in the study area between the altitude of 850 and 1000 hPa is defined as the adjusted value (the computing method for anthropogenic temperature is discussed in Appendix B). In accordance with Equation (B2), the temperature tendency of four upper-air stations at the altitude of 850 hPa is adjusted to the altitude of 1000 hPa, in which it can indicate the surface natural temperature variability. The adjusted values are then distributed to 31 conventional weather stations based on the distance. As shown in Equation (B1), the difference between actual measured temperature and surface natural temperature in 2002 is defined as anthropogenic temperature.

5. Modelling strategies

Correlations between climate, land cover and human factors within a large and rapidly developing urbanized ecosystem have been shown (Unger *et al*., 2001; Zhou *et al*., 2004; Chen *et al*., 2006; Du *et al*., 2007; Jenerette *et al*., 2007; Tonkaz and Centin, 2007; Xiao and Weng, 2007; O'Neil and Ebi, 2009; Yilmaz *et al*., 2009). Based on the OMR method, the Fractional Step Regression method is used to test the spatial correlations between anthropogenic temperature and the two anthropogenic factors, land use and population.

5.1. Anthropogenic temperature-population (ATP) model

Univariate nonlinear regression analysis is used to reveal the relationship between population density and anthropogenic temperature for each month in the study area. Four kinds of models, linear, logarithmic, inverse and power, are tested to fit the data. To achieve the best fit, the model with a maximum R square (determination coefficient) is selected as the ATP model.

5.2. Anthropogenic temperature-land use (ATL) model

Different land use patterns characterized by the area ratio of land-use types may lead to different thermal environments. The ATL model describes the relationship between the area ratio of land-use types and anthropogenic temperature.

The residual error sequence of the ATP model is regarded as the proportion of variability not explained by population. To facilitate research and place emphasis on the main factors, a principal components regression model was constructed based on principal components analysis (PCA). The relationship between residual error and area ratio of each land-use type was verified by testing the linear, logarithmic, inverse and power models with the maximum R-square. Based on the component matrix, the principal components regression model was then transformed to the ATL model, which takes residual error as a dependent variable and the area ratio of land-use types as independent variables.

In the process of PCA, the first three common factors are extracted. The cumulative contribution rate of these factors is around 80% of the total variance, which represents the combination of land-use types. Multiple linear regression was performed with the common factors and residual error. The Durbin-Watson (DW) and F-tests were performed to determine whether the relationship is linear and whether the residual error sequence is an autocorrelation. Based on the component matrix, the regression equation was revised to ensure that the independent variables are the original area ratio of eight land-use types if the DW and F-tests are passed. Equation (3) shows the process of standardization. Equation (4) is the ATL model:

$$L'_j = \frac{f(L_j) - A_j}{\sigma_j} \qquad (3)$$

$$Y = \sum_{j=1}^{8} \left(\sum_{i=1}^{3} a_i X_{ij} \right) \times L'_j \qquad (4)$$

L'_j is the independent variable representing the area ratio of land-use types after standardization; L_j denotes the independent variable representing the original area ratio of land-use types; $f(L_j)$ represents the nonlinear relationship in the model; A_j is the mean value of the samples; σ_j is the standard deviation of the samples; Y

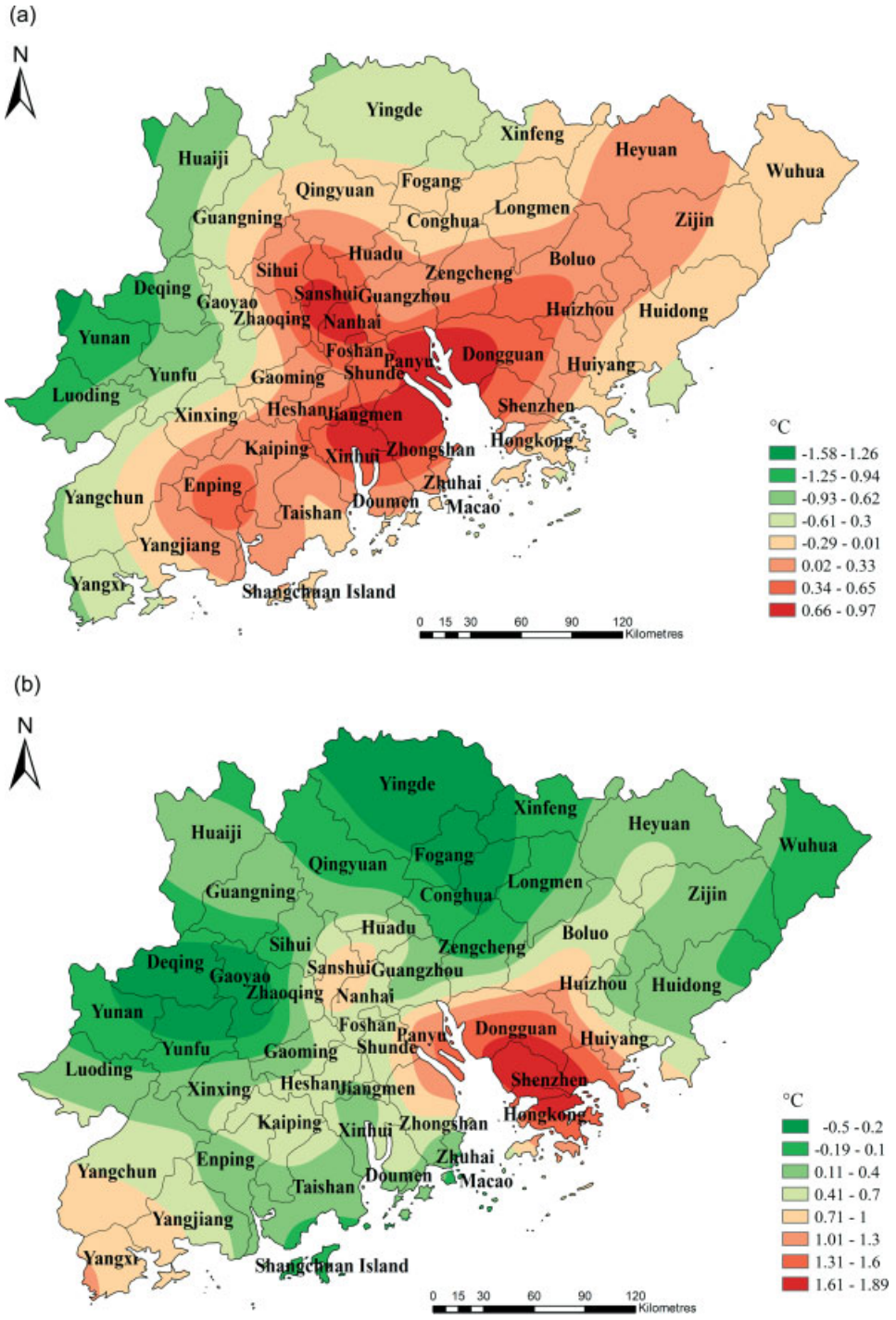

Figure 4. Spatial distribution of anthropogenic temperature in the daytime (a) and at night (b). The data of anthropogenic temperature are interpolated to raster using spline function.

is the residual error, that is, the proportion of anthropogenic temperature not explained by population; a_i is the regression coefficient and $X(i, j)$ is the component matrix.

After the models were constructed, the different contributions of land-use types to anthropogenic temperature was analysed by comparing the regression coefficients from the models. The reasons for seasonal and diurnal variations are then explored. Many factors affect anthropogenic temperature, but only land use pattern and population are considered to build ATP and ATL models applicable to the area of PRD.

6. Results and discussion

6.1. Spatial ratio of land-use types and population density

According to the calculation results of area ratio, the majority of the study area is covered by woodland and paddy field, with an average ratio of around 65%. The

Table I. ATP models in the daytime and at night all the year round.

Month	Time	ATP model	Model type	R square
January	Day	$Y = 0.0002x - 0.2884$	Linear	0.1324
	Night	$Y = 0.0004x - 0.5627$	Linear	0.2917
February	Day	$Y = -80.07/x + 5.265$	Inverse	0.134
	Night	$Y = -165.734/x + 3.55$	Inverse	0.304
March	Day	$Y = 0.6048x^{0.0955}$	Power	0.0363
	Night	$Y = 0.466lnx - 2.607$	Logarithmic	0.4043
April	Day	$Y = 0.0566lnx + 2.2825$	Logarithmic	0.0135
	Night	$Y = 0.4014lnx - 0.7904$	Logarithmic	0.6356
May	Day	$Y = 0.7237x^{0.1507}$	Power	0.2243
	Night	$Y = 0.5177lnx - 2.3708$	Logarithmic	0.6736
June	Day	$Y = 0.2852lnx - 0.8238$	Logarithmic	0.2
	Night	$Y = 0.0004x + 0.4588$	Linear	0.4924
July	Day	$Y = -140.591/x - 0.068$	Inverse	0.228
	Night	$Y = 0.0003x - 0.2467$	Linear	0.4768
August	Day	$Y = 0.1033lnx - 0.4887$	Logarithmic	0.0312
	Night	$Y = 0.0002x - 0.4046$	Linear	0.3531
September	Day	$Y = -90.158/x - 0.762$	Inverse	0.158
	Night	$Y = 0.0003x + 0.1879$	Linear	0.29
October	Day	$Y = 0.5016lnx - 4.8841$	Logarithmic	0.5411
	Night	$Y = 0.0004x - 1.3185$	Linear	0.3572
November	Day	$Y = -151.857/x - 3.597$	Inverse	0.258
	Night	$Y = 0.0001x - 0.9595$	Linear	0.0229
December	Day	$Y = -104.999/x - 1.826$	Inverse	0.203
	Night	$Y = 123.927/x - 0.325$	Inverse	0.131
Annual	Day	$Y = 0.2254lnx - 1.2337$	Logarithmic	0.3509
	Night	$Y = 0.0003x + 0.1323$	Linear	0.4468

R square stands for determination coefficient; Y for anthropogenic temperature; x for population density.

area ratio of arid land and urban land is about 6 and 9%, respectively. Grassland and rural residence have almost the same ratio of 1.2% on average. Sea only exists in the eight coastal units.

Figure 3 shows that the population density in this area is quite high, especially around the Pearl River estuary where there are 4000–6000 people km^{-2}.

6.2. Spatial distribution of anthropogenic temperature

Figure 4(a) and (b) show the spatial distribution of anthropogenic temperature during the day and at night using the data of annual average anthropogenic temperature.

During the day the anthropogenic temperature is high around the Pearl River estuary, especially in Zhongshan, Xinhui, Dongguan, Panyu, Nanhai and Sanshui, because more factories release heat and there are greater amounts of urban construction work and human activities in the area. The anthropogenic temperature decreases with the increasing distance from the estuary.

At night, the spatial pattern of anthropogenic temperature is different. Anthropogenic temperature is highest on the east side of the estuary, especially in Dongguan, Shenzhen and Hong Kong. It is also high in Nanhai, Sanshui and west of Yangjiang, possibly because of the status of land use.

6.3. The relationship between population density and anthropogenic temperature

The results in Table I indicate a positive correlation between population density and anthropogenic temperature. Linear relationships are evident at night, whereas logarithmic and inverse relationships are dominant in the daytime. Approximately 83% of the relationship models are statistically significant at the significance level of 95%. Figure 5(a)–(d) show the raw data and fitted relationships using the four models. For each case, the fitted curve yields the maximum R square.

6.4. The relationship between the area ratio of land-use types and anthropogenic temperature

Table II shows the relationship between the first three common factors in PCA and the residual error of the ATP model. It also demonstrates the ATL model, through which the F test is passed, at the same time the DW test is passed or to be determined. The principal components X_1, X_2, and X_3 in Table II show different information on land-use types. The main information on paddy field, woodland, grassland, water, urban land and rural residence is represented by variable X_1, and the majority information on arid land is shown by X_3, while the dominant information on sea is embodied by X_2. The relationships between land-use types and

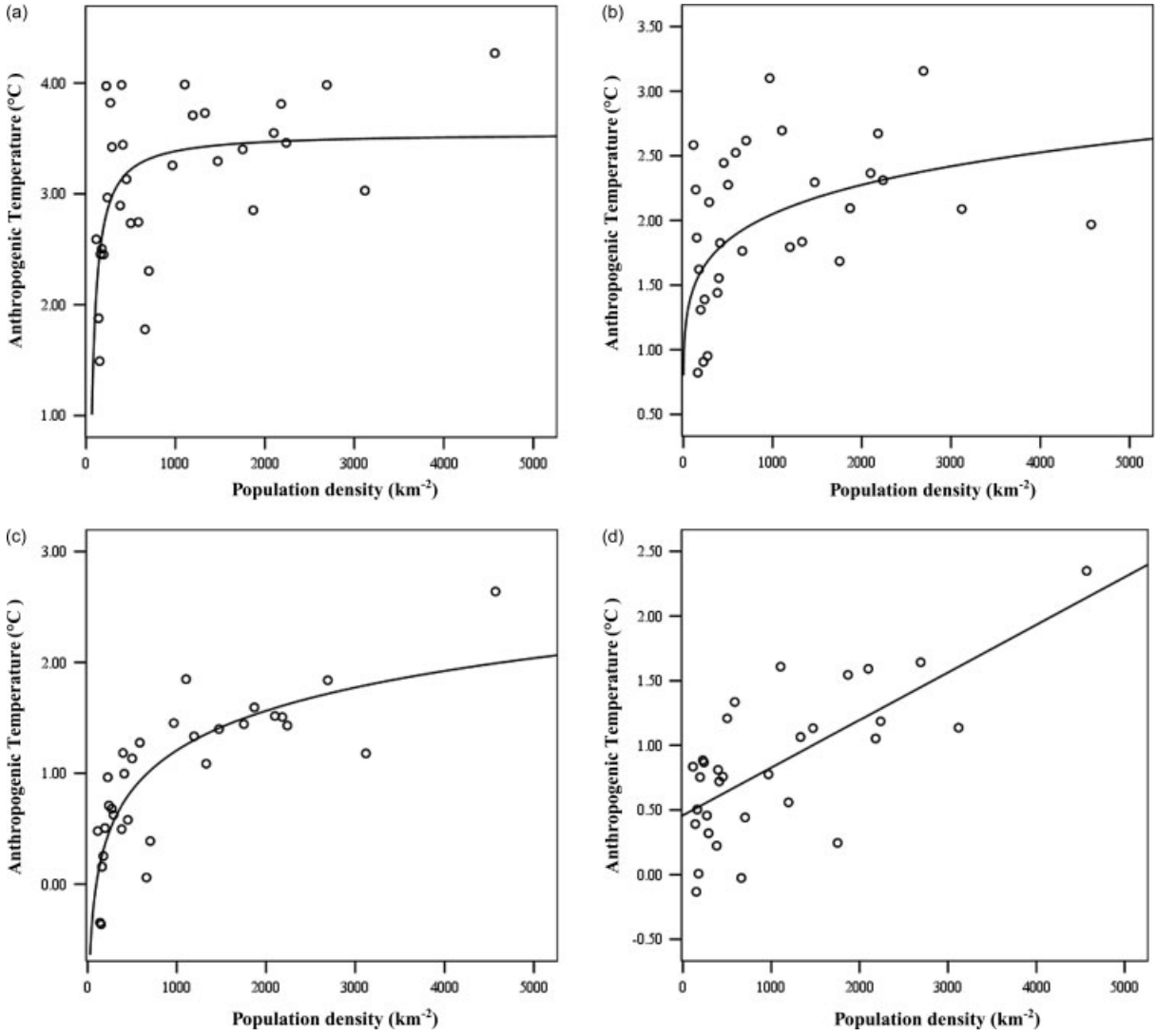

Figure 5. Four kinds of models describing the correlations between population density and anthropogenic temperature: (a) The inverse model at night in February: $y = -165.734/x + 3.55$. (b) The power model in the daytime in May: $y = 0.7237 \times 0.1507$. (c) The logarithmic model at night in May: $y = 0.5177lnx - 2.3708$. (d) The linear model at night in June: $y = 0.0004x + 0.4588$. Solid line: model results; circles: observed values.

anthropogenic temperature are strong from February to June and in November: temperature is closely related to land use in spring and autumn. This is because there is no dominant large-scale weather system in transition seasons and atmospheric circulation is not as active as it is in summer and winter. Urban land, arid land and water bodies have positive effects on temperature increase, whereas woodland has a negative effect, regardless of time of day.

High heat capacity and impermeable surfaces in urban land lead to more heat storage and air warmth because these raise heat absorption and lower heat consumption. In addition, tall buildings increase surface roughness, thus reducing the rate of ventilation in urban areas (Lin *et al*., 2008). Preferential heating in the city compared to the surrounding area also increases convection over the city that traps heat (as well as pollutants) inside the urban area (Oke, 1982; Arnfield, 2003). However, the effect of urban land on temperature is not obvious, mostly because old cities in the estuary, such as Guangzhou and Foshan, do not show a rapid increase in urban land as they have no land to develop further, having already expanded fully in the 1990s (Weng, 2002). Arid land is located on the hillside that belongs to a transition zone from paddy field to woodland. It has low vegetation coverage and, thus, low humidity, which acts as a heat source causing a higher energy absorption than consumption (Sailor, 1995; Jiang *et al*., 2007; Zhang *et al*., 2009). Water bodies in this area exist as rivers, reservoirs and canals, all of which are line-shaped. Thus, the small water body area prevents the heat of upper air from dissipating. On the other hand, woodland lowers air temperature resulting from transpiration of plants (Tian *et al*., 2005). Grassland and sea have a negative effect on the increase of surface air temperature during the day and a positive effect at night.

The relationship between grassland and temperature is the strongest as the regression coefficient of grassland

Table II. Principal components regression models and ATL models in the daytime and at night all the year round.

Month	Time	Principal components regression model	DW	F	ATL model
January	Day	$R = -0.02 - 0.104X_1 + 0.015X_2 - 0.143X_3$	Y	N	
	Night	$R = -0.012 + 0.025X_1 - 0.068X_2 + 0.248X_3$	Y	N	
February	Day	$R = 0.105X_1 - 0.21X_2 + 0.093X_3$	TBD	Y	$R = 0.327 - 0.033/L_1 + 1.882L_2 + 0.008/L_3 - 3.178L_4 + 1.169L_5 + 0.101lnL_6 + 4.715L_7 - 1.213L_8$
	Night	$R = -0.013X_1 + 0.27X_2 + 0.307X_3$	TBD	Y	$R = 0.12 - 1.426L_1 + 4.08L_2 - 0.748L_3 + 20.75L_4 + 0.069lnL_5 + 0.456L_6 + 6.529L_7 + 1.411L_8$
March	Day	$R = 0.127 - 0.121X_1 + 0.021X_2 - 0.046X_3$	N	N	
	Night	$R = -0.007X_1 + 0.188X_2 + 0.241X_3$	Y	Y	$R = -0.226 + 0.028/L_1 + 2.05L_2 - 0.589L_3 + 13.553L_4 + 0.028lnL_5 - 0.001/L_6 + 5.169L_7 + 1.368L_8$
April	Day	$R = 6.35\text{E-}07 + 0.19X_1 - 0.273X_2 - 0.047X_3$	Y	Y	$R = 0.345 - 0.049/L_1 - 0.003/L_2 + 0.009/L_3 - 13.74L_4 + 1.714L_5 + 1.031L_6 + 7.164L_7 - 1.776L_8$
	Night	$R = 0.111X_1 + 0.039X_2 + 0.174X_3$	Y	Y	$R = 0.037 + 0.024/L_1 + 0.108lnL_2 + 0.176L_3 + 15.796L_4 + 0.001/L_5 - 0.911L_6 - 7.708L_7 + 0.569L_8$
May	Day	$R = 0.074 - 0.066X_1 - 0.194X_2 + 0.171X_3$	TBD	Y	$R = 0.355 - 0.033/L_1 - 0.001/L_2 + 0.352L_3 - 11.871L_4 + 0.726L_5 + 0.0003/L_6 - 2.176L_7 - 1.399L_8$
	Night	$R = 0.019X_1 - 0.183X_2 + 0.149X_3$	Y	Y	$R = -0.33 + 0.018/L_1 + 2.944L_2 - 0.095L_3 + 15.422L_4 - 0.001/L_5 - 0.001/L_6 - 3.809L_7 + 0.576L_8$
June	Day	$R = 0.225X_1 - 0.25X_2 - 0.178X_3$	TBD	Y	$R = 0.864 - 0.059/L_1 - 0.002/L_2 + 0.009/L_3 - 20.376L_4 + 1.825L_5 + 0.097lnL_6 + 5.894L_7 - 1.881L_8$
	Night	$R = -0.033 - 0.019X_1 + 0.148X_2 + 0.042X_3$	Y	N	
July	Day	$R = 0.054X_1 + 0.058X_2 + 0.04X_3$	N	N	
	Night	$R = 0.002 - 0.015X_1 + 0.047X_2 + 0.101X_3$	Y	N	
August	Day	$R = -6.8\text{E-}05 + 0.094X_1 + 0.112X_2 - 0.019X_3$	TBD	N	
	Night	$R = 0.035 + 0.067X_1 - 0.056X_2 + 0.034X_3$	Y	N	
September	Day	$R = 0.051X_1 - 0.069X_2 + 0.11X_3$	Y	N	
	Night	$R = -0.027 + 0.055X_1 - 0.159X_2 + 0.044X_3$	TBD	N	
October	Day	$R = 0.082X_1 + 0.091X_2 - 0.012X_3$	Y	N	
	Night	$R = -0.007 - 0.068X_1 - 0.199X_2 + 0.026X_3$	Y	N	
November	Day	$R = 9.97\text{E-}06 + 0.101X_1 + 0.292X_2 + 0.192X_3$	TBD	Y	$R = -0.591 + 0.047/L_1 + 0.003/L_2 - 0.382L_3 + 14.207L_4 - 0.0002/L_5 + 0.001/L_6 - 0.453L_7 + 2.061L_8$
	Night	$R = 0.013 + 0.160X_1 - 0.345X_2 + 0.136X_3$	Y	Y	$R = 0.422 + 0.007/L_1 - 0.004/L_2 + 0.471lnL_3 + 22.713L_4 - 0.095lnL_5 + 0.0004/L_6 - 23.033L_7 - 1.38L_8$
December	Day	$R = 0.012X_1 + 0.128X_2 + 0.082X_3$	TBD	N	
	Night	$R = -0.02X_1 - 0.264X_2 + 0.077X_3$	Y	N	
Annual	Day	$R = 5.48\text{E}{-}05 - 0.073X_1 - 0.079X_2 + 0.056X_3$	Y	N	
	Night	$R = -0.011 - 0.026X_1 - 0.049X_2 + 0.17X_3$	Y	Y	$R = -0.099 - 0.085L_1 + 2.907L_2 + 0.017L_3 + 10.188L_4 + 0.031lnL_5 + 0.019lnL_6 - 2.811L_7 - 0.297L_8$

DW stands for Durbin-Watson test; F for F-test; R for the residual error of ATP model (that is anthropogenic temperature excluding population factor); X_2 and X_3 for principal components representing the arid land, paddy field and sea, while X_1 for principal component representing other land use types; L_1 for paddy field; L_2 for arid land; L_3 for woodland; L_4 for grassland; L_5 for water body; L_6 for urban land; L_7 for rural residence; L_8 for sea. Y indicates the test is passed; N indicates not passed; TBD indicates to be determined.

with anthropogenic temperature is the highest. Grasslands are mainly located in the central area of large cities, such as Shenzhen and Hong Kong, or are interspersed among woodlands. In the daytime, latent heat of grassland vapourization takes up a large portion of the heat budget which leads to temperature decrease, but at night the heat stored in the dense plant canopy increases the temperature (Wang *et al*., 2007). Thus, based on Figure 4(b), more grassland in the east of the estuary, especially in Shenzhen, may contribute to higher temperature at night. Sea has a negative effect on the temperature increase in the daytime, which can explain why anthropogenic temperature is higher in the north of the estuary than in the coastal area (Figure 4(a)). Although no wind data were obtained during this study, it is inferred that the interactive mechanism of the effect of sea on temperature is the sea-land breeze causing thermal exchange. Cool, moist wind blows from the sea to the land, bringing down the temperature of the coastal region in the daytime. However, warm, dry wind blows from the land to the sea, thus increasing temperature at night (Fan and Guo, 1998; Chen *et al*., 2009).

Paddy field mixing crop with water is an important land-use type that increases temperature in the daytime but reduces it at night. According to Figure 4(a) and (b), it may cause higher temperature in the daytime and lower temperature at night in areas with larger paddy fields west of the estuary. Temperature in the surrounding areas changes noticeably with the exploitation and use of paddy fields. A model for the water temperature in paddy fields has been developed (Kuwagata *et al*., 2008), but hardly any research has focused on the relationship between paddy fields and the air temperature above. Recent studies (Yokohari *et al*., 1997, 2001) revealed that an irrigated paddy field reduces the daytime air temperature in summer. This result is in contrast to the conclusion of this study, which may be explained by the particularity of this area. However, it is still difficult to amplify the effect of paddy field with the current data analysis. Future work is needed to combine other hydrothermal conditions in the PRD region.

Rural residence has a positive effect on temperature increase in February and a negative effect in May and November. The correlation is weak because rural residences in the PRD region are scattered and the area they occupy is small.

The results can be used to predict the pattern of human energy consumption and help industrial sectors arrange industrial patterns reasonably. These can also be used to guide the optimization of land use and city planning. Inferring from the ATL models and learning from some research findings (Yang *et al*., 2009), improving the woodland area around the Pearl River estuary can effectively mitigate anthropogenic temperature. In addition, planting paddy fields mixed with grasslands is a good practice to balance day and night temperatures. The government also needs to reinforce regulations on field management to prohibit illegal land exploitation, including digging canals and ditches without permission, enclosing tidelands for cultivation and wasting land resources in the form of abandoned land resulting from deforestation and illegal construction.

To understand the relationship between land-use types and anthropogenic temperature in this region better, the complicated thermodynamic mechanism must be addressed in future studies.

7. Conclusions

Preliminary results show that using statistical approaches and the idea of spatialization is desirable for establishing models of anthropogenic temperature and human dimensions, which are likely to be applicable to the coastal urbanized area in Southern China.

Anthropogenic temperature is high around the Pearl River estuary in the daytime, and decreases with the increase in distance from the estuary. At night, temperature is highest on the east side of the estuary.

The relationships between population density and anthropogenic temperature are mainly linear at night and logarithmic or inverse in the daytime.

Anthropogenic temperature is closely related to land use in spring and autumn. Relationships between anthropogenic temperature and land-use types are different based on the thermal characteristics of the underlying surfaces. Arid land, water bodies, and urban land have a positive effect on temperature increase, whereas woodland has a negative effect, regardless of time of day. Grassland and sea have a negative effect in the daytime and a positive effect at night, whereas paddy field increases the temperature in the daytime but reduces it at night. Rural residence does not show a clear impact.

Acknowledgements

This research was supported by the key project of the National Natural Science Foundation of China (40635028). The authors would like to acknowledge the Chinese Academy on Environmental Planning for providing the data on land use. All climate data are available for use in the Guangdong Meteorological Bureau, China (GDMB); the National Centres for Environmental Prediction, USA (NCEP); and the National Centre for Atmospheric Research, USA (NCAR).

Appendix A: Data Specification.

According to statistics from China Meteorological Administration, the average space between every two national meteorological surface observing stations is 61 km. Thus, 30 km is chosen as the radius of every control unit. In the late 1990s, automatic observation stations were set up with the development of information technology. However, data from automatic observation are only taken as the reference for manual readings because their accuracy has not been validated.

All stations located in an open and ventilated field are equipped with maximum and minimum thermometers 1.5 m over the ground. Thermometer readings represent daily maximum and minimum temperatures and are measured once in 2000 Beijing time (that is, 1200 UTC) every day.

All data undergo strict quality control by the National Meteorological Information Centre of China Meteorological Administration. Errors from measurement, relocation, and other reasons are corrected, and all the datasets are homogenized. The stations involved are all national meteorological observation units, where the quality of data is highest. However, altitude was not taken into account because most of the stations are on a similar level, between 10 and 30 m.

Appendix B: Computing Method of Anthropogenic Temperature.

$$AT = T_{2002} - (T_{1980} + NT) \tag{B1}$$

AT is the anthropogenic temperature; T_{2002} denotes the temperature of conventional weather stations in 2002; T_{1980} is the temperature of conventional weather stations in 1980; and NT is the surface natural temperature variability from 1980 to 2002:

$$NT = 2.2 \times \{UTIR_{850\text{hPa}} + (NTIR_{1000\text{hPa}} - NTIR_{850\text{hPa}})\} \tag{B2}$$

NT is the surface natural temperature variability from 1980 to 2002; $UTIR_{850\text{hPa}}$ represents the temperature tendency at the altitude of 850hPa of the upper-air stations from 1980 to 2005; $NTIR_{1000\text{hPa}}$ is the temperature tendency at the altitude of 1000hPa of the grid point (22.5 °N, 112.5 °E) in NCEP R-2 data from 1980 to 2005; and $NTIR_{850\text{hPa}}$ denotes the temperature tendency at the altitude of 850hPa of the grid point (22.5 °N, 112.5 °E) in NCEP R-2 data from 1980 to 2005:

$$UTIR_{850\text{hPa}} = 10 \times \frac{\sum(t_i - t_a) \times (T_i - T_a)}{\sum(t_i - t_a)^2} \quad i = 1, 2, \ldots, n)\} \tag{B3}$$

$UTIR_{850\text{hPa}}$ is the temperature tendency at the altitude of 850 hPa of the upper-air stations from 1980 to 2005 representing temperature variation every 10 years; t_i denotes the serial number of the time series; t_a is the mean value of serial numbers; T_i represents the temperature at the altitude of 850 hPa of upper-air stations in the period of 1980 to 2005; T_a is the mean value of T_i and n is a constant ($n = 26$) representing the number of years.

The methods of computing $NTIR_{1000\text{hPa}}$ and $NTIR_{850\text{hPa}}$ are similar to those of $UTIR_{850\text{hPa}}$.

References

Arnfield AJ. 2003. Two decades of urban climate research: a review of turbulence, exchanges of energy and water, and the urban heat island. *International Journal of Climatology* **23**: 1–26.

Chen XL, Feng YR, Li JN, Lin WS, Fan SJ, Wang AY. 2009. Numerical simulations on the effect of sea-land breezes on atmospheric haze over the Pearl River Delta region. *Environmental Modeling and Assessment* **14**: 351–363.

Chen XL, Zhao HM, Li PX, Yin ZY. 2006. Remote sensing image-based analysis of the relationship between urban heat island and land use/cover changes. *Remote Sensing of Environment* **104**: 133–146.

Du Y, Xie ZQ, Zeng Y, Shi YF, Wu JG. 2007. Impact of urban expansion on regional temperature change in the Yangtze River Delta. *Journal of Geographical Sciences* **17**: 387–398.

Fan YZ, Guo LX. 1998. The climate suitability of tourism at the coastline destinations of China. *Journal of Natural Resources* **13**: 304–311.

Fan SJ, Wang AY, Fan Q, Liu J, Wang BM. 2005. Atmospheric boundary layer concept model of the Pearl River Delta and its application. *Journal of Tropical Meteorology* **21**: 286–292.

Harlan SL, Brazel AJ, Prashad L, Stefanov WL, Larsen L. 2006. Neighborhood microclimates and vulnerability to heat stress. *Social Science Medicine* **63**: 2847.

Hessman-Konsaris A. 1998. *Wplyw pogody na samopoczucie*. Diogenes: Warszawa, Poland.

Jenerette GD, Hanlan SL, Brazel A, Jones N, Larsen L, Stefanov WL. 2007. Regional relationships between surface temperature, vegetation, and human settlement in a rapidly urbanizing ecosystem. *Landscape Ecology* **22**: 353–365.

Jiang XY, Zhang CL, Gao H, Miao SG. 2007. Impacts of urban albedo change on urban heat island in Beijing – a case study. *Acta Meteorologica Sinica* **65**: 301–307.

Jin M, Dickinson RE, Zhang DL. 2005. The footprint of urban areas on global climate as characterized by MODIS. *Journal of Climate* **18**: 1551–1565.

Kalnay E, Cai M. 2003. Impact of urbanization and land-use change on climate. *Nature* **423**: 528–531.

Kalnay E, Cai M, Li H, Tobin J. 2006. Estimation of the impact of land-surface forcings on temperature trends in eastern United States. *Journal of Geophysical Research* **111**: 1–13.

Karl TR, Diaz HF, Kukla G. 1988. Urbanization: its detection and effect in the United States climate record. *Journal of Climate* **1**: 1099–1123.

Kuwagata T, Hamasaki T, Watanabe T. 2008. Modeling water temperature in a rice paddy for agro-environmental research. *Agricultural and Forest Meteorology* **148**: 1754–1766.

Lim YK, Cai M, Kalnay E, Zhou LM. 2005. Observational evidence of sensitivity of surface climate changes to land types and urbanization. *Geophysical Research Letters* **32**: L22712.

Lin CY, Chen WC, Liu SC, Liou YA, Liu GR, Lin TH. 2008. Numerical study of the impact of urbanization on the precipitation over Taiwan. *Atmospheric Environment* **42**: 2934–2947.

Oke TR. 1973. City size and the urban heat island. *Atmospheric Environment* **7**: 769–779.

Oke TR. 1982. The energetic basis of the urban heat island. *Quarterly Journal of the Royal Meteorological Society* **108**: 1–24.

O'Neil MS, Ebi KL. 2009. Temperature extremes and health: impacts of climate variability and change in the United States. *American College of Occupational and Environmental Medicine* **51**: 13–25.

Piotrowicz K. 2009. The occurrence of unfavorable thermal conditions on human health in central Europe and potential climate change impacts: an example from Cracow, Poland. *Environmental Management* **44**: 766–775.

Rosenthal JP, Jessup CM. 2009. Global climate change and health: developing a research agenda for the NIH. *Transportation America Clinic Climatology Associate* **120**: 129–141.

Sailor DJ. 1995. Simulated urban climate response to modifications in surface albedo and vegetative cover. *Journal of Applied Meteorology* **34**: 1694–1704.

Stanhill GJ, Kalma D. 1995. Solar dimming and urban heating at HongKong. *International Journal of Climatology* **15**: 933–941.

Tian Z, Zhu N, Liu JJ. 2005. Relationship between heat island effect and artificial factors. *Journal of Tianjin University* **38**: 830–833.

Tonkaz T, Centin M. 2007. Effects of urbanization and land-use type on monthly extreme temperatures in a developing semi-arid region, Turkey. *Journal of Arid Environments* **68**: 143–158.

Unger J, Sümeghy Z, Gulyás Á, Bottyán Z, Mucsi L. 2001. Land-use and meteorological aspects of the urban heat island. *Meteorological Applications* **8**: 189–194.

Wang XX, Hu YM, Liu X, Gao FF, Zhu QJ. 2007. Microclimatic modification of urban grassland in Beijing. *Journal of Guangxi Normal University: Natural Science Edition* **25**: 23–27.

Weng Q. 2001. A remote sensing-GIS evaluation of urban expansion and its impact on surface temperature in the Zhujiang Delta, China. *International Journal of Remote Sensing* **22**: 1999–2014.

Weng QH. 2002. Land use change analysis in the Zhujiang Delta of China using satellite remote sensing, GIS and stochastic modelling. *Journal of Environmental Management* **64**: 273–284.

Xiao HL, Weng QH. 2007. The impact of land use and land cover changes on land surface temperature in a karst area of China. *Journal of Environmental Management* **85**: 245–257.

Yang XC, Zhang YL, Liu LS, Zhang W, Ding MJ, Wang ZF. 2009. Sensitivity of surface air temperature change to land types in China. *Science in China Series D: Earth Sciences* **52**: 1207–1215.

Yilmaz S, Toy S, Yildiz ND, Yilmaz H. 2009. Human population growth and temperature increase along with the increase in urbanization, motor vehicle numbers and green area amount in the sample of Erzurum city, Turkey. *Environmental Monitoring and Assessment* **148**: 205–213.

Yokohari M, Brown RD, Kato Y, Moriyama H. 1997. Effects of paddy fields on summertime air and surface temperatures in urban fringe areas of Tokyo, Japan. *Landscape Urban Plan* **38**: 1–11.

Yokohari M, Brown RD, Kato Y, Yamamoto S. 2001. The cooling effect of paddy fields on summertime air temperature in residential Tokyo, Japan. *Landscape Urban Plan* **53**: 17–27.

Zhang HQ, Gao XJ, Li YH. 2009. Climate impacts of land-use change in China and its uncertainty in a global model simulation. *Climate Dynamics* **32**: 473–494.

Zhou LM, Dickinson RE, Tian YH, Fang JY, Li QX, Kaufmann RK, Tucker CJ, Myneni RB. 2004. Evidence for a significant urbanization effect on climate in China. *Proceedings of the National Academy of Sciences* **101**: 9540–9544.

